

WATER AND DUST EMISSION FROM W HYDRAE

VICTOR ZUBKO¹ AND MOSHE ELITZUR

Department of Physics and Astronomy, University of Kentucky, Lexington, KY 40506-0055

Revised, September 20, 2000

ABSTRACT

We construct a self-consistent model for the wind around W Hya by solving the coupled equations describing the hydrodynamics and dust radiative transfer problems. The model matches simultaneously the observed continuum radiation and wind velocity profile. The water line emission is calculated next using the water abundance as the only free parameter, fitted from the ISO observations of Neufeld et al. (1996) and Barlow et al. (1996). The gas temperature is determined from a thermal balance calculation that includes water as one of its main components. Our model successfully fits all the observed water lines, resolving a major discrepancy between the modeling results of the two observing teams. The mass loss rate is $2.3 \times 10^{-6} M_{\odot} \text{ yr}^{-1}$, the water abundance is 1.0×10^{-4} and the ortho:para ratio is 1:1.3.

Subject headings: stars: AGB and post-AGB — stars: individual: W Hya — infrared: stars — circumstellar matter — dust, extinction — molecular processes

1. INTRODUCTION

Water is a dominant coolant of outflows around cool oxygen-rich stars (Goldreich & Scoville 1976, GS hereafter; Chen & Neufeld 1995, CN hereafter; Truong-Bach et al 1999, TB hereafter). However, until recently observations of water cooling lines were impossible because of the atmospheric opacity at these wavelengths. The situation has changed with the successful launch of the Infrared Space Observatory (ISO). One of the first objects observed with ISO was W Hydrae, an M7.5 semi-regular red giant, and it showed the expected thermal water emission in observations with both the SWS (Neufeld et al 1996; hereafter N96) and LWS instruments (Barlow et al 1996; hereafter B96). Both teams also fitted their observations based on the GS approach, resulting in strikingly different estimates for the mass loss rate: $6 \times 10^{-7} M_{\odot} \text{ yr}^{-1}$ (B96) and $(0.5-3) \times 10^{-5} M_{\odot} \text{ yr}^{-1}$ (N96). Here we aim to resolve this discrepancy. In contrast with the original studies we construct a self-consistent model of the radiation field, dust, and gas in the shell, taking account of all the infrared continuum observations as an additional constraint.

2. MODELING

The driving force of the wind is radiation pressure on the dust, the gas particles are dragged along by collisions with the dust grains. The internal properties of the gas, such as temperature, do not play any role in the dynamics, the wind structure can be obtained by solving the coupled equations for hydrodynamics and dust radiative transfer. We now describe our calculation for W Hya. With the derived model we proceed to solve the H₂O level population problem.

2.1. Dynamics and IR Emission

A complete calculation of the wind structure requires a solution of the coupled hydrodynamics and dust radiative transfer problems. Traditionally these calculations

involved a large number of input parameters. However, Ivezić & Elitzur (1995) noted that the dusty wind problem possesses general scaling properties such that, for a given type of grains, both the dynamics and radiative transfer depend primarily on a single parameter – the overall optical depth. Subsequent analysis by Ivezić & Elitzur (1997) established rigorously that the dust radiative transfer problem possesses scaling properties under the most general circumstances. Scaling was incorporated in the code DUSTY² (Ivezić et al. 1999), which solves fully the dusty wind problem. The solution provides the radial variation of the velocity and radiation fields in terms of the scaled distance $y = r/R_{\text{in}}$, where R_{in} is the shell inner boundary. That boundary is defined by the condition $T_c = T_{\text{dust}}(y = 1)$, where T_c is the dust condensation temperature. The actual value of R_{in} never enters.

We use for modeling “astronomical silicate” dust grains with optical constants from Laor & Draine (1993) and the power law size distribution of Mathis et al. (1977). We assume prompt dust formation at $y = 1$ and no further grain growth or destruction. The only input parameter in addition to the dust properties is the stellar temperature $T_* = 2500$ K (Haniff et al. 1995). From a series of DUSTY models in which we varied the visual optical depth τ_V , the temperature T_c and the shell outer radius $Y = R_{\text{out}}/R_{\text{in}}$ we chose the one that best fits all the observations all the way from 1 μm to 1.2 mm; because of its irregular variability, optical data is not included. We find that models with $\tau_V = 0.7-1.0$, $T_c = 900-1100$ K and $Y > 1000$ are almost equally successful in reproducing the observational spectrum. The most significant parameter by far is τ_V ; T_c has only a small effect on the fitting and the role of Y is marginal. The model with $\tau_V = 0.83$, $T_c = 1000$ K and $Y = 12,000$ minimizes the fitting errors and is presented in Fig. 1. Matching the model flux to observations in scale as well as spectral shape determines the shell angular dimensions (Ivezić & Elitzur 1997). The shell inner diameter is $0''.182$, consistent with the measured stellar diameter $0''.046$ (Han-

¹On leave from the Main Astronomical Observatory, National Academy of Sciences, Kiev, Ukraine

²Accessible at <http://www.pa.uky.edu/~moshe/dusty>

iff et al. 1995), and its outer diameter $36'$, in agreement with the IRAS observations of Hawkins (1990).

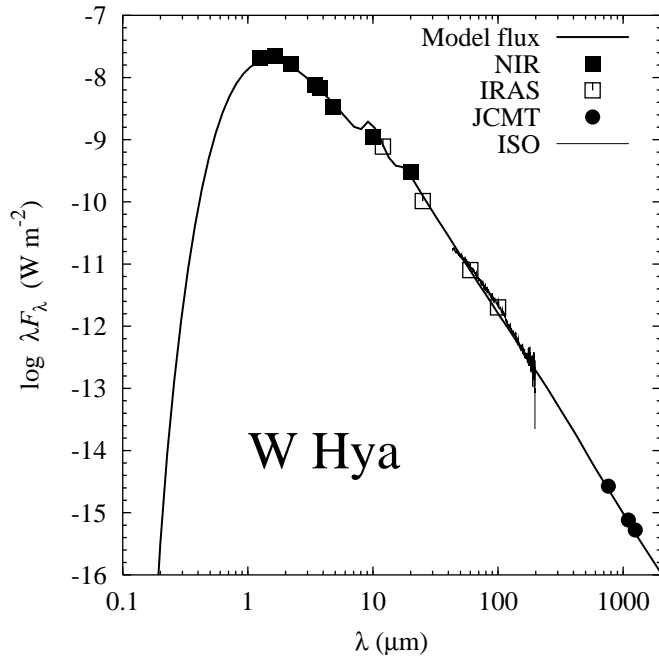


FIG. 1.— The spectral energy distribution of W Hya. Data indicated by filled squares (NIR) are from Wilson et al. (1972); open squares (IRAS) from Hawkins (1990); filled circles (JCMT) from van der Veen et al. (1995) and Walmsley et al. (1991). The thin solid line shows the ISO data of Barlow et al. (1996). The bold solid line is our model result.

2.2. Water Lines

The statistical rate equations for the water level populations require the following input: the radiation field, to determine radiative excitations; the gas density and temperature, for the collision rates; and the water column density, required for the line radiative transfer (Elitzur 1992). DUSTY's output provides the radiation field as well as the dimensionless velocity and density profiles in the shell. Fixing the scale of densities requires two additional input properties. We take the distance $d = 115$ pc from the Hipparcos catalog. This sets $R_{\text{in}} = 1.6 \times 10^{14}$ cm and $R_{\text{out}} \sim 1$ pc, and the luminosity is $11,050 L_{\odot}$ in agreement with Haniff et al. (1995). Next, the wind terminal velocity $v_e = 8$ km s^{-1} (Young 1995) fixes the velocity scale and determines the gas-to-dust mass ratio $r_{\text{gd}} = 850$ and the mass-loss rate $\dot{M} = 2.3 \times 10^{-6} M_{\odot} \text{ yr}^{-1}$. The complete velocity profile is shown in figure 2 together with the data for OH and H_2O masers as well as CO thermal emission. All are properly explained by the model results. The SiO data is displaced from the wind velocity profile, as expected for this maser's location inside the dust formation zone (cf Elitzur 1992).

The only required input quantities that remain unknown are the gas temperature and water abundance, and we fit those simultaneously from the water line observations. We calculate the temperature from the balance of cooling and heating due to adiabatic expansion, grain-gas collisions and H_2O rovibrational transitions (we estimate the H_2 vibrational contribution and find it negligible). We solve for the populations of the lowest 45 rotational levels of the ground vibrational state of ortho- and para-

water; this accounts for all levels with energy $\lesssim 2000$ K above ground. The molecular data are from the HITRAN database (Rothman et al. 1998), the collision rate coefficients from Green et al. (1993). The level populations and line emissivities are calculated with the escape probability method as functions of distance r , and the line fluxes by integrating the line emissivities over the shell volume. The free parameters are the abundances of the two water species, which must be considered independently since there is no radiative coupling between them. Detailed modeling shows that these abundances are constant in the region where the water emission originates (CN, TB). Because of the central role of H_2O in the energy balance, the calculations of the temperature and water line emission are coupled, and repeated until the best fit achieved for the line observations. The best fit is found for water abundance $n(\text{H}_2\text{O})/n(\text{H}_2) = 1.0 \times 10^{-4}$ and the ratio ortho:para = 1:1.3. Figure 3 shows the temperature profile. The model parameters are summarized in Table 1, results and comparison with observations in Table 2.

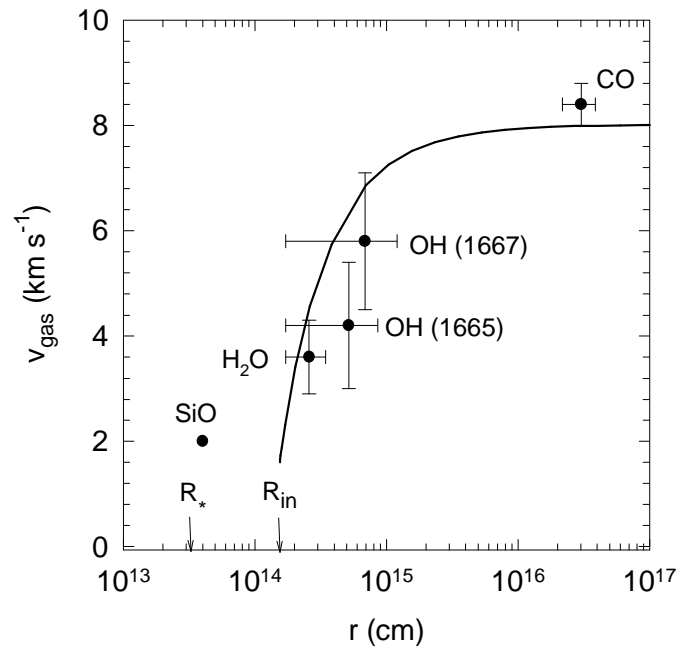


FIG. 2.— The model prediction for the gas velocity profile. Data points (from Szymczak et al, 1998) show the H_2O and OH maser and CO thermal emission from the wind. The SiO maser emission originates in the extended atmosphere.

3. DISCUSSION

Our model fits all the water lines within the observational errors, which generally exceed 50%. The quality of the fit for the LWS data is comparable to that of the B96 model. For the SWS data N96 present a range of models for each line, and our model fits that data set better than any single one of them. Therefore, our model resolves the conflict among the previous water line calculations, fitting all the data with a single value for the mass loss rate. It is important to note that \dot{M} is determined by the infrared data and v_e , and remains unchanged during the modeling of the water lines. We find that the acceptable range of \dot{M} is $\sim 2-3 \times 10^{-6} M_{\odot} \text{ yr}^{-1}$, with a nominal value of $2.3 \times 10^{-6} M_{\odot} \text{ yr}^{-1}$. Except for the high-end of the N96

range, most estimates of \dot{M} are in agreement with ours within the errors (cf N96 and references therein).

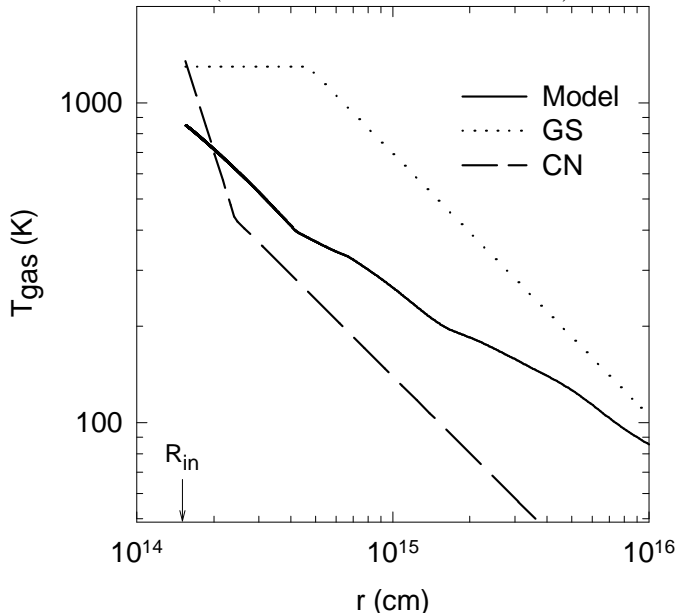


FIG. 3.— The gas temperature profile from our best-fit model. Shown are also power-law fits for the Goldreich & Scoville (GS) and Chen & Neufeld (CN) temperature profiles.

The source of the large discrepancy with N96 is not clear. Neufeld et al suggest that the temperature profile could be the reason, but this does not seem to be the case. Our temperature profile is not that different from the CN profile, which was used in the N96 study, especially in the relevant range $T \gtrsim 400$ K (figure 3). We compared the various contributions to heating and cooling with those listed by CN and Neufeld & Kaufman (1993), and find good agreement; the difference in resulting profiles can be attributed to the different parameters used in the two calculations (CN used $\dot{M} = 3 \times 10^{-5} M_{\odot} \text{ yr}^{-1}$). The two profiles differ much more with the GS profile employed in the B96 model, which produced \dot{M} similar to ours. We suspect that a more important source of difference could be the radiation field, since radiative excitations play an important role in the water population distribution. A comparison is impossible since N96 do not give details of the radiation field they employed. A proper radiation field appears crucial for the water line calculations.

The uncertainty in fitted parameters depends on the particular observations that constrain them. We estimate that the acceptable range for r_{gd} is $\sim 850 \pm 100$. We experimented with both power-law and single-size ($a = 0.1 \mu\text{m}$) grain distributions and found the differences negligible. The large uncertainties in the measured line fluxes translate into a large uncertainty in the abundances of the two species of water. Between the two, the para- H_2O abundance is subject to the larger uncertainty and can vary by as much as factor 3, so that the ortho:para ratio can be anywhere from 1 to 1/3. By comparison, B96 obtained 1 for this ratio. All of these results differ greatly from the thermodynamic limit of 3. Depending on the ortho:para ratio, we find acceptable models for $n(\text{H}_2\text{O})/n(\text{H}_2)$ in the range $\sim 1-4 \times 10^{-4}$.

In the modeling efforts of both B96 and N96, \dot{M} was one of numerous free parameters fitted from the water line

observations. The scaling approach taken here reduces the number of free parameters to the essential minimum and determines \dot{M} prior to the water line fitting. Table 1 breaks the model parameters into three categories. Quantities in the first division are specified as input, in addition to the IR and water observations. The second group includes the free parameters of our two fitting procedures while the third group lists results derived from our fits. Given grain properties, the IR observations are fitted with the three free parameters τ_V , T_c and Y and the single independent input T_* . The resulting model determines also the dimensionless velocity profile. Adding as independent input the source distance and the wind final velocity, the model results determine the full velocity profile, and τ_V determines also \dot{M} and the gas-to-dust ratio. Fitting the water lines involves no other input and only two free parameters — the ortho- and para-water abundances. Thanks to the central role of water lines in the gas temperature calculation, the gas temperature is determined self-consistently as part of this second fitting procedure. Since the only free parameters in fitting the observed water fluxes are the abundances of the two species, confidence in the derived values is greatly enhanced. In principle, we could have used \dot{M} as a free parameter in the water calculations, as in the previous studies. In that case, consistency between the results of the two fitting procedures would be used as an additional constraint, automatically met by our calculation.

While radiation pressure on the dust grains is generally accepted as the driving mechanism behind the wind expansion, this mechanism has not been fully tested. The solutions of radiative transfer and the hydrodynamics problems must result in the same parameters, but this fundamental test has not been performed thus far; self-consistent modeling of both the IR emission and the wind structure in the same source has not yet been attempted. The most detailed previous calculation we are aware of is the TB modeling of R Cas. However, in that work the radiation field was not calculated self-consistently, instead it was derived from a dust temperature profile that was assumed beforehand as an input property. In contrast, DUSTY determines this temperature from a proper calculation of radiative equilibrium coupled to the radiative transfer including dust scattering, absorption and emission. The spectral energy distribution is fitted with just three free parameters, only one of which (τ_V) is significant. Once these parameters are set, the outflow terminal velocity determines the entire velocity profile without any more freedom in the model. It is highly significant that a single self-consistent model with the minimal necessary number of parameters provides agreement with both the spectral energy distribution and the molecular velocity observations. Apart from resolving the \dot{M} discrepancy in W Hya, the success of our model provides strong support for the basic paradigm of winds in late-type stars.

We thank Michael Barlow for the ISO LWS spectrum of W Hya, David Neufeld for help with the water molecular data, Željko Ivezić for his comments on the manuscript and the referee for useful suggestions and for pointing out the Hipparcos distance measurement. The partial support of NASA and NSF is gratefully acknowledged.

REFERENCES

- Barlow, M.J., et al. 1996, A&A, 315, L241 (B96)
 Chen, W., & Neufeld, D.A. 1995, ApJ, 453, L99 (CN)
 Elitzur, M. 1992, Astronomical Masers, Dordrecht: Kluwer
 Goldreich, P., & Scoville, N. 1976, ApJ, 205, 144 (GS)
 Green, S., Maluendes, S., & McLean, A.D. 1993, ApJS, 85, 181
 Haniff, C.A., Scholz, M., & Tuthill, P.G. 1995, MNRAS, 276, 640
 Hawkins, G.W. 1990, A&A, 229, L5
 Ivezić, Ž., & Elitzur, M. 1995, ApJ, 445, 415
 Ivezić, Ž., & Elitzur, M. 1997, MNRAS, 287, 799
 Ivezić, Ž., Nenkova, M., & Elitzur, M. 1999, User Manual for DUSTY, University of Kentucky Internal Report
 Laor, A., & Draine, B.T. 1993, ApJ, 402, 441
 Mathis, J.S., Rumble, W., & Nordsieck, K.H. 1977, ApJ, 217, 425
 Neufeld, D.A., & Kaufman, M.J. 1993, A&A, 418, 263
 Neufeld, D.A., et al. 1996, A&A, 315, L237 (N96)
 Rothman, L.S., et al. 1998, JQSRT, 60, 665
 Szymczak, M., Cohen, R.J., & Richards, A.M.S. 1998, MNRAS, 297, 1151
 Truong-Bach, et al. 1999, A&A, 345, 925 (TB)
 van der Veen, W.E.C.J., Omont, A., Habing, H.J., & Matthews, H.E. 1995, A&A, 295, 445
 Walmsley, C.M., Chini, R., Steppe, H., Forveille, T., & Omont, A. 1991, A&A, 248, 555
 Wilson, W.J., Schwatz, P.R., Neugebauer, G., Harvey, P.M., & Becklin, E.E. 1972, ApJ, 177, 523
 Young, K., 1995, ApJ, 445, 872

TABLE 1
 MODEL PARAMETERS

<i>Input parameters:</i>	
Stellar temperature ^a	2500 K
Distance ^b	115 pc
Final velocity ^c	8 km s ⁻¹
<i>Fitting parameters:</i>	
Optical depth at 0.55 μm ^I	0.83
Dust temperature at R_{in} ^I	1000 K
Shell thickness (R_{out}/R_{in}) ^I	12,000
H ₂ O abundance at R_{in} ^w	1.0×10^{-4}
ortho-H ₂ O:para-H ₂ O ^w	1:1.3
<i>Derived parameters:</i>	
Stellar radius	3.9×10^{13} cm
Stellar luminosity	11,050 L_{\odot}
Shell inner radius (R_{in})	1.6×10^{14} cm
Mass loss rate	2.3×10^{-6} M_{\odot} yr ⁻¹
Gas-to-dust mass ratio	850
Shell outer radius (R_{out})	1.2 pc
Dust temperature at R_{out}	17 K

^a Haniff et al. (1995)

^b Hipparcos Catalog

^c Young (1995)

^I fitted from IR observations

^w fitted from H₂O lines

TABLE 2
OBSERVED AND MODEL FLUXES OF H₂O LINES

λ (μm)	Transition	$F_{\text{mod}}^{\text{a}}$	$F_{\text{obs}}^{\text{a}}$	$\frac{F_{\text{mod}}}{F_{\text{obs}}}$
180.486	o: 2 ₂₁ →2 ₁₂	3.43	2.90	1.18
179.527	o: 2 ₁₂ →1 ₀₁	12.48	8.66	1.44
174.624	o: 3 ₀₃ →2 ₁₂	8.31	9.21	0.90
156.265	o: 5 ₂₃ →4 ₃₂	2.42	5.41	0.45
144.517	p: 4 ₁₃ →3 ₂₂	5.57	6.38	0.87
132.408	o: 4 ₂₃ →4 ₁₄	2.97	5.50	0.54
125.356	p: 4 ₀₄ →3 ₁₃	12.39	16.60	0.75
113.538	o: 4 ₁₄ →3 ₀₃	11.27	17.40	0.65
108.073	o: 2 ₂₁ →1 ₁₀	15.47	13.00	1.19
89.989	p: 3 ₂₂ →2 ₁₁	18.11	27.30	0.66
83.283	p: 6 ₀₆ →5 ₁₅	14.42	22.60	0.64
78.742	o: 4 ₂₃ →3 ₁₂	14.08	28.00	0.50
67.089	p: 3 ₃₁ →2 ₂₀	17.80	59.80	0.30
66.438	o: 3 ₃₀ →2 ₂₁	18.45	22.90	0.81
63.458	p: 8 ₀₈ →7 ₁₇	12.99	30.40	0.43
58.699	o: 4 ₃₂ →3 ₂₁	15.35	19.50	0.79
57.637	p: 4 ₂₂ →3 ₁₃	30.13	36.20	0.83
40.691	o: 4 ₃₂ →3 ₀₃	36.07	23.00	1.57
31.772	o: 4 ₄₁ →3 ₁₂	39.95	63.00	0.63
29.837	o: 7 ₂₅ →6 ₁₆	30.72	32.00	0.96
37.984	o: 4 ₄₁ →4 ₁₄	13.19	28.00	0.47 ^b

Note. — Ortho transitions are marked by “o”, para by “p”. The 57–180 μm lines are from Barlow et al. (1996), the 29–41 μm lines from Neufeld et al. (1996). ^aFluxes are in 10^{-20} W cm⁻². ^bThis line is severely contaminated by blending with two others.